MAGNETOHYDRODYNAMICS Vol. 59 (2023), No. 3-4, pp. 415–424
DOI: 10.22364/mhd.59.3-4.13

ELECTROMAGNETIC CONTROL OF THE DIRECT STRIP CASTING PROCESS

V. Dzelme[1*], *A. Jakovičs*[1], *E. Baake*[2]

[1] *Institute of Numerical Modelling, University of Latvia, Jelgavas str. 3, Riga, Latvia*
[2] *Institute of Electrotechnology, Leibniz University Hannover, Wilhelm-Busch street 4, Hannover, Germany*
[*] *e-Mail: valters.dzelme@lu.lv*

Controlling the melt flow and free surface motion is crucial to maintain stability of many metallurgical processes. In the direct strip casting process, a known problem is the back-flow of liquid metal into the small gap between the moving belt and the refractory. Apart from geometrical and feeding modifications reported in the literature to reduce the back-flow, electromagnetic technologies could potentially solve this issue. We investigate numerically the application of AC magnetic field to deflect the melt from the back-flow area. Simulations show that it is possible to completely prevent the back-flow but at the expense of introducing oscillations in the shape of the cast solid sheet downstream. Combination of AC field for back-flow prevention with static (DC) magnetic field for free surface stabilization downstream can provide a fully stable casting process.

Introduction. The belt casting process is being developed by multiple research groups under different names, such as Horizontal Single Belt Casting (HSBC) and Direct Strip Casting (DSC). The DSC abbreviation is used in the paper. A thorough review of the belt casting and similar technologies can be found in [1], [2].

In the DSC process, a liquid metal is poured onto a moving belt, which is intensively cooled from the bottom and goes through an area of inert gas atmosphere to protect the alloy from oxidation and contamination. The melt is contained on the belt by copper blocks on both sides that move together with the belt. The liquid metal solidifies into a solid strip that is continuously pulled away for further processing and coiling. Typical cast materials are steel [3] and aluminium alloys [4].

Laboratory-based research casters are usually small, e.g., a belt width of 75 mm [5] or 160 mm [6]. The first commercial belt caster for steel was launched in Germany in 2012 [7]. The cast strips are 1 m wide and 15 mm thick, pulled at around 24 m/min [8]. For comparison, older technologies, such as Thin Slab Casting [9], cast 50 – 60 mm thick strips at 5 m/min [10], which requires considerably more secondary processing.

There are several stability issues in the belt casting process. One is that liquid metal can flow not only in the direction of the belt movement but also into the small gap between the belt and the bottom of the refractory [11]. If the melt solidifies inside the gap, it can damage the equipment. A stable meniscus can form if the gap is very small (less than 1 mm) [12]. However, stability of the meniscus depends on the physical properties of the melt and other factors. The back-flow can be reduced by creating an inclined refractory [4], which decreases the impact of liquid metal on the belt.

Another problem in DSC is that non-uniform flow velocities and free surface oscillations affect the final strip thickness profile. One solution reported for belt casting is blowing argon jets against the liquid metal to spread the melt uniformly across the belt [3]. Another option is to use the electromagnetic (EM) interaction. For example, the use of travelling magnetic field to modify the flow has already been reported for DSC [3].

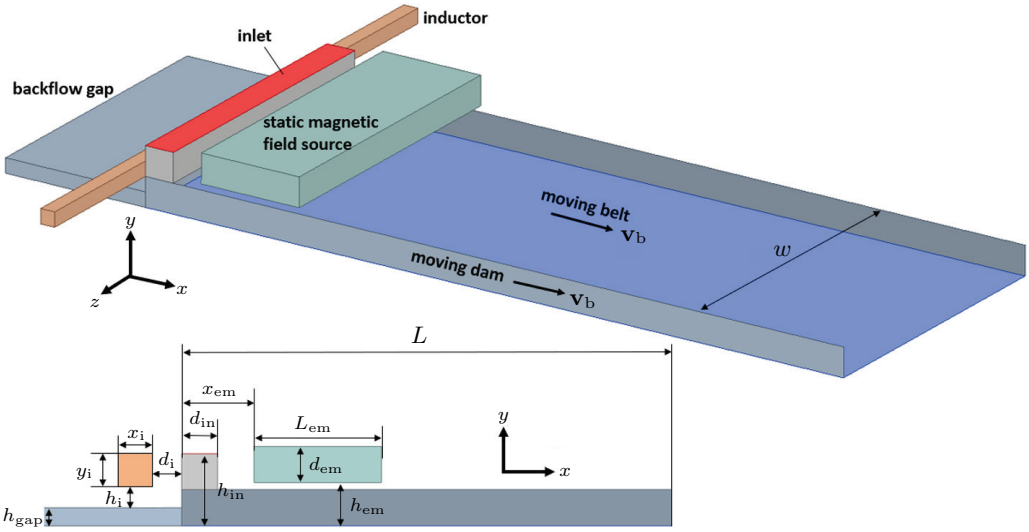

Fig. 1. Scheme of the belt casting model.

In a related technology, the Twin Roll Casting, the use of an EM dam to contain liquid metal has been reported in [13]. We investigate a similar approach for the belt casting.

In our previous work [14], we have shown that, depending on the liquid metal layer's thickness, a stable deflection of the melt away from an AC inductor can be achieved. In this work, we investigate numerically the application of AC and DC magnetic fields to prevent the back-flow and stabilize the free surface downstream.

1. Numerical model.

All simulations are done using the open-source software *Elmer* (electromagnetics) [15] and *OpenFOAM* (fluid flow, heat transfer, solidification) [16], which are coupled using the *EOF-Library* [17]. This software combination has succesfully been applied for the simulation of liquid metal stirring by rotating permanent magnets [18], [19], EM levitation [20] and liquid metal free surface waves induced by a low-frequency pulsed magnetic field [21] and a low-frequency AC magnetic field [22].

Scheme of the belt casting model is shown in Fig. 1. The liquid metal is poured down from a gap in the refractory, spreads onto the moving belt and gradually solidifies. Two EM systems are considered – a straight high-frequency inductor near the back-flow area and a DC magnetic field system above the belt. The inductor is supposed to keep the liquid metal from entering the gap. The static field is used to decelerate the fast flowing liquid metal, distributing it evenly across the belt and helping to obtain a more uniform solid strip at the outlet.

The cast metal is aluminium with the melting point of $T_s = 933\,\mathrm{K}$. The material properties are assumed constant (independent of temperature and the same for liquid and solid phases): density $\rho = 2311\,\mathrm{kg/m^3}$, viscosity $\mu = 0.8\,\mathrm{mPa{\cdot}s}$, electrical conductivity $\sigma = 3.70\,\mathrm{MS/m}$, surface tension $\gamma = 0.84\,\mathrm{N/m}$, thermal conductivity $\lambda = 98\,\mathrm{W/(m{\cdot}K)}$, heat capacity $c_p = 1122\,\mathrm{J/(kg\ K)}$, latent heat $L_T = 360\,\mathrm{kJ/kg}$. These are the values for liquid aluminium at 1200 K [23]. The gas phase has physical properties of the air.

1.1. OpenFOAM. The *OpenFOAM* model is based on the `interFoam` solver that simulates a turbulent incompressible two-phase flow with free surface capturing using the Volume of Fluid (VOF) [24] method, with an additional implementation of the temper-

ature equation and solidification. The two phases represented by the VOF method are liquid metal and gas.

Solidification is implemented to affect only the liquid metal phase. The approach is based on the enthalpy-porosity method, such as described in [25]. The basic idea is that the liquid fraction function β_T is introduced to be equal to 1 in liquid and to 0 in solid. Using the error function, it can be defined as $\beta_\mathrm{T} = 0.5\mathrm{erf}\left(a_\mathrm{T}(T - T_\mathrm{s})\right) + 0.5$, where a_T is a constant, T is the temperature and T_s is the melting point. This method is normally applied to simulate a two-phase system with liquid and solid, without gas. In a three-phase system with gas, the liquid fraction for gas must always be 1. Conveniently, using the volume fraction α that is zero in gas and 1 in the other material (liquid and solid metal), the total liquid fraction can be written as $\beta = 1 + \alpha(\beta_\mathrm{T} - 1)$. In addition, since the interface between gas and metal (both liquid and solid) described by α is centered at 0.5 and is not perfectly sharp, to have more control over the behaviour of β near the metal-gas interface, in the β expression α can be replaced by a function $\beta_\alpha = 0.5\mathrm{erf}\left(b_\mathrm{T}(\alpha - \alpha_0)\right) + 0.5$, where b_T is a steepness coefficient and α_0 is the value where the function is centered. Note that α is modified only in the calculation of the liquid fraction and not in the VOF model. The liquid fraction β implemented in this work is

$$\beta = 1 + (0.5\mathrm{erf}\left(b_\mathrm{T}(\alpha - \alpha_0)\right) + 0.5)(0.5\mathrm{erf}\left(a_\mathrm{T}(T - T_\mathrm{s})\right) + 0.5 - 1). \tag{1}$$

The solidification model contains several numerical constants (α_0, a_T, b_T) that must be optimized for a specific case. In belt casting, the solidified material must move steadily with the belt speed while also preserving its shape (deformation of the solid is not considered). A test case to find the optimal values was a rectangular solid block ($T < T_\mathrm{s}$ everywhere in the domain) moving with a constant speed in the gas atmosphere. The optimal values that provide no visible smearing of the solid/gas interface were found to be $\alpha_0 = 0.04$, $a_\mathrm{T} = 4$, $b_\mathrm{T} = 100$. For other casting configurations the optimal values can be different.

Finally, β is used in the momentum equation to make the liquid metal flow temperature-dependent. If $T < T_\mathrm{s}$, the liquid metal should behave as if it is solid, i.e. either completely static or, in the case of belt casting, moving with the belt speed. This is achieved by a momentum source term

$$\mathbf{f}_\mathrm{solid} = A_0 \frac{(1-\beta)^2}{\beta^3 + \epsilon} \left(\mathbf{v}_\mathrm{b} - \mathbf{v}\right), \tag{2}$$

where $\mathbf{v}$ is the flow velocity, $\mathbf{v}_\mathrm{b}$ is the belt speed, A_0 is the mushy zone constant (a large number like 10^5) and ϵ is a small number (like 10^{-3}).

The implemented approach is basically a pseudo three-phase model, where gas is always fluid, but the other material can take two states – liquid and solid. This considerably simplifies things because from the computational fluid dynamics standpoint the model still has only two phases – liquid metal and gas, with liquid metal having some temperature-dependent properties to make it behave like solid below the melting point.

The *OpenFOAM* model contains the region above the moving belt with liquid/solid metal, inlet and outlet, and some gas. To considerably simplify the model and reduce the simulation time, radiation and natural convection are ignored. A typical magnitude of the heat flux through the cooled belt is $\sim 10^7\,\mathrm{W/m^2}$ [2]. Assuming the upper value of the emissivity ~ 1, the radiative heat flux from the surface at 1200 K to the environment at 300 K is of the order of $10^5\,\mathrm{W/m^2}$, which is two orders of magnitude lower than the

Table 1. Boundary conditions in the *OpenFOAM* model. $\mathbf{v}_\mathrm{b}$ – belt speed, p – pressure, k – turbulent kinetic energy, ω – turbulent eddy frequency, ν_t – eddy viscosity, α – volume fraction, T – temperature, θ – contact angle, ϕ_v – electric scalar potential, WF – wall functions.

	belt/dam	other surfaces	inlet	back-flow gap and outlet
$\mathbf{v}$	$\mathbf{v}=\mathbf{v}_\mathrm{b}$	$\mathbf{v}=0$	$\mathbf{v}=\mathbf{v}_\mathrm{in}=\mathrm{const}$	$\partial\mathbf{v}/\partial n=0$ (for outflow) $\mathbf{v}=0$ (for inflow)
p	$\partial p/\partial n=0$	$\partial p/\partial n=0$	$\partial p/\partial n=0$	$p_\mathrm{static}=0$
α	$\theta_\mathrm{b}=\mathrm{const}$	$\theta_d=180^o$	$\alpha=1$	$\alpha=0$ (for inflow) $\partial\alpha/\partial n=0$ (for outflow)
T	$\partial T/\partial n=\mathrm{const}$	$\partial T/\partial n=0$	$T=T_\mathrm{in}$	$\partial T/\partial n=0$
k	WF	WF	$k=10^{-3}\,\mathrm{m}^2/\mathrm{s}^2$	$k=10^{-3}\,\mathrm{m}^2/\mathrm{s}^2$ (inflow) $\partial k/\partial n=0$ (outflow)
ω	WF	WF	$\omega=1\,\mathrm{s}^{-1}$	$\omega=1\,\mathrm{s}^{-1}$ (inflow) $\partial\omega/\partial n=0$ (outflow)
ν_t	WF	WF	calculated from k and ω	calculated from k and ω
ϕ_v	$\partial\phi_\mathrm{v}/\partial n=0$	$\partial\phi_\mathrm{v}/\partial n=0$	$\partial\phi_\mathrm{v}/\partial n=0$	$\partial\phi_\mathrm{v}\partial n=0$

flux through the cooled belt. Natural convection in the liquid metal can be ignored due to a relatively small thickness of the melt layer ($\sim 10\,\mathrm{mm}$), and convection of the gas phase has very little influence on the motion of the melt due to the small density.

The k-ω SST DES model was used for turbulence. The *OpenFOAM* simulation is transient. The time-step Δt is controlled by the Courant number condition $\mathrm{Co}=v\Delta t/\Delta x<1$, where Δx is the mesh element size. The boundary conditions in *OpenFOAM* are summarized in Table 1. For simplicity, the cooling boundary condition on the belt is a constant heat flux $\mathbf{q}_\mathrm{belt}$. In *OpenFOAM*, this must be set using a temperature gradient, which is the heat flux divided by the heat conductivity. For a specified contact angle, *OpenFOAM* calculates $\partial\alpha/\partial n$ and uses it as a boundary condition for the α equation solved in the VOF method.

A representative mesh is shown in Fig 2 (bottom). The mesh is structured with a characteristic size of elements near the back-flow area around 1 mm.

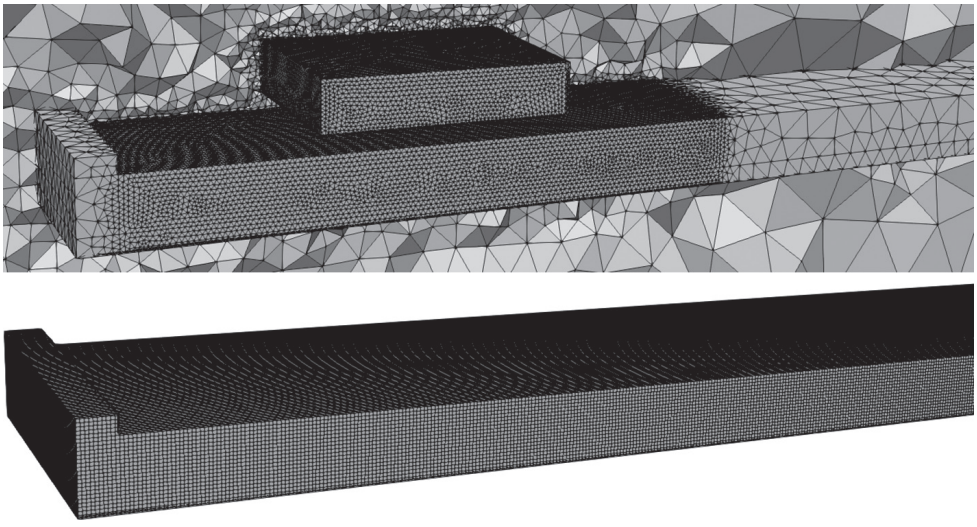

Fig. 2. Examples of the numerical mesh for *Elmer* (top) and *OpenFOAM* (bottom).

1.2. Elmer. The *Elmer* model contains the melt region, an inductor, a DC field source and the surrounding gas. The inductor is made as a straight rectangular rod with a constant current density across its cross-section. In the static field case, the magnetic field source (magnetization M) is specified in a box above the melt layer as $M_y = M_0$. If the static field source is a permanent magnet with a remanence B_r, $M_0 = B_r/\mu_0$. The boundary condition in *Elmer* in both cases is the magnetic vector potential $\mathbf{A} = 0$ at the external boundary. The case with the inductor is solved in a frequency domain using the `WhitneyAVHarmonicSolver`, whereas the case with static magnetic field is using `WhitneyAVSolver` (magnetostatics).

A representative mesh is shown in Fig. 2 (top). The mesh is tetrahedral with a characteristic size of elements near the back-flow area around 1 mm.

1.3. Coupling. Two models are considered in this work. One with only the AC inductor and the other with the AC inductor and DC field. With the first model, *OpenFOAM* uses the Lorentz force calculated by *Elmer* and EM fields are recalculated in *Elmer* whenever the condition $\max(\Delta\alpha) > 0.5$ is true anywhere in the *OpenFOAM* domain.

With the combined AC inductor and DC magnetic field, a simulation without the AC inductor is run first to obtain the DC field and transfer it to *OpenFOAM*. After that, a simulation with the AC inductor is run. In addition to using the AC Lorentz force calculated by *Elmer*, *OpenFOAM* solves an equation for the electric potential using the magnetic field distribution $\mathbf{B}$ calculated by *Elmer* to account for the $\mathbf{v} \times \mathbf{B}$ term. This approach, which is described in more detail in [18], is valid for the magnetic Reynolds number $\mathrm{Rm} < 1$. In belt casting, taking width of the belt w and the belt speed v_b as the characteristic length and velocity, respectively, $\mathrm{Rm} = \sigma\mu_0 v_\mathrm{b} w < 0.1$. The Lorentz force used by *OpenFOAM* is, therefore, the sum of the AC part calculated in *Elmer* and the DC part due to the $\mathbf{v} \times \mathbf{B}$ term calculated in *OpenFOAM*. The DC magnetic field stays constant throughout the simulation, but the AC field (and the corresponding Lorentz force) is recalculated according to the condition $\max(\Delta\alpha) > 0.5$.

2. Results.

Since aluminium is one of the typical cast materials in belt casting, it is considered in this work. The physical properties of aluminium at 1200 K are given above. The contact angle between the liquid metal and the belt depends on the specific materials, surface characteristics (roughness), temperature, etc. The belt is typically made of either steel or copper [3]. On a copper substrate, the liquid aluminium has a dynamic contact angle from 105 to 140 degrees [12]. For simplicity, the constant contact angle is set on the belt $\theta_\mathrm{belt} = 140°$. The contact angle to the moving side dam is set to $\theta_{dam} = 180°$, and to other surfaces (refractory) to 135°.

The geometrical parameters are (see Fig. 1): $h_\mathrm{gap} = 0.5$ cm, $L_\mathrm{b} = 50$ cm, $w = 10$ cm, $h_\mathrm{in} = 2.5$ cm, $d_\mathrm{in} = 1$ cm, $h_\mathrm{em} = 2.5$ cm, $x_\mathrm{em} = 6$ cm, $d_\mathrm{em} = 1.5$ cm, $L_\mathrm{em} = 7$ cm, $x_i = y_i = 0.5$ cm, $h_i = 0.2$ cm, $d_i = 1$ cm. The casting conditions are $v_\mathrm{in} = 20$ cm/s, $T_\mathrm{in} = 1200$ K, $v_\mathrm{b} = 20$ cm/s. The cooling heat flux is $q_\mathrm{belt} = -13.8\,\mathrm{MW/m^2}$.

The first simulation was done without any EM stabilization. The distribution of liquid/solid phases during the first moments of casting is shown in Fig. 3. The belt is moving from left to right in the figure. Clearly, $h_\mathrm{gap} = 5$ mm is enough for the melt to flow into the gap, where it starts solidifying. Since the entire solidified metal is set to move with the belt, at some point in time the metal has solidified throughout the gap height. At that point the solid metal together with the liquid metal is pulled out of the gap until it reaches the area directly below the inlet, and then a fresh liquid metal is again allowed

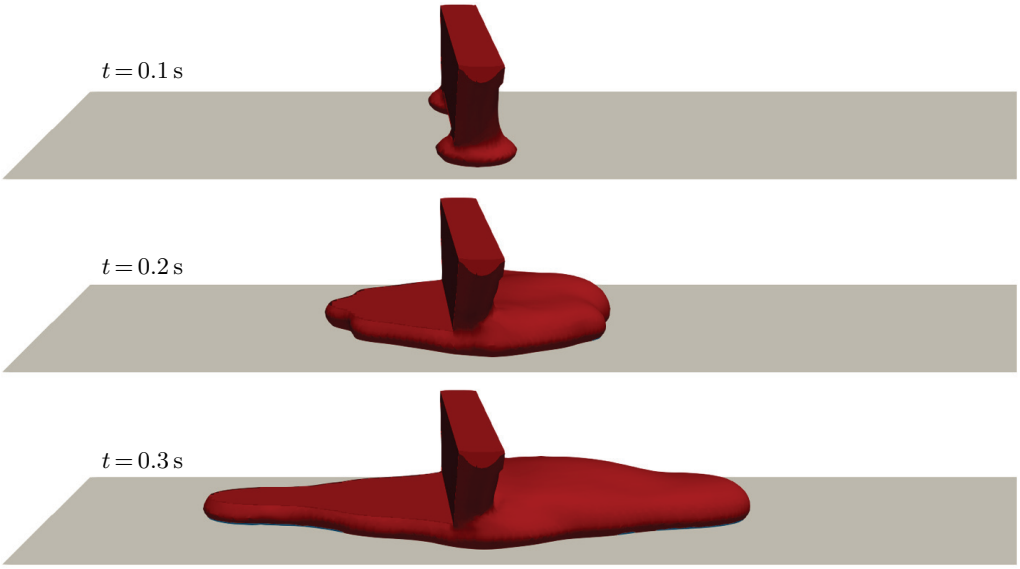

Fig. 3. Liquid/solid phases during the first 0.3 s of casting without EM stabilisation: (left) full view and (right) cross-section; red – liquid, blue – solid.

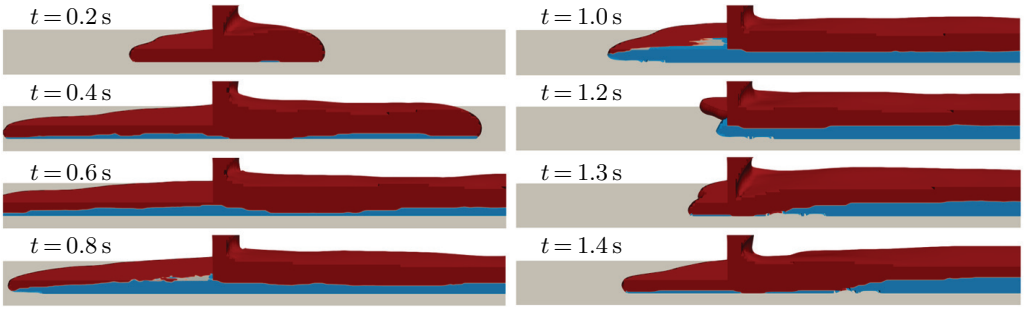

Fig. 4. Phases in the middle cross-section during the first 1.4 s without EM stabilisation; red – liquid, blue – solid.

to flow into the gap. Fig. 4 demonstrates this effect by showing the phase distribution in a vertical cross-section. This is detrimental to the uniformity of the cast strip.

There are several possible solutions reported in the literature, such as using an inclined refractory and optimizing the feeding system [4]. It could be possible to control the back-flow using EM technologies. The main idea here is to use AC magnetic field of a straight inductor to deflect the liquid metal from there. Considering the properties of liquid aluminium and the results of our previous study [14], one can expect a relatively stable deflection of the melt layer with the thickness $h_{\text{gap}} = 5$ mm.

After several test simulations with different inductor currents, a stable deflection was achieved with the inductor current $I = 1$ kA and frequency $f = 4$ kHz. The time behavior in the first moments of casting with the AC field is illustrated in Fig. 5. The back-flow is completely prevented and no free surface instabilities are observed. However, some small surface perturbations travel downstream, where they disturb the casting process.

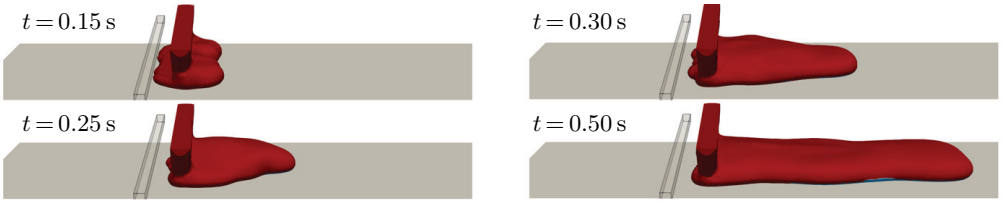

Fig. 5. Phases during the first 0.5 s with the AC field, current $I = 1$ kA, frequency $f = 4$ kHz; red – liquid, blue – solid.

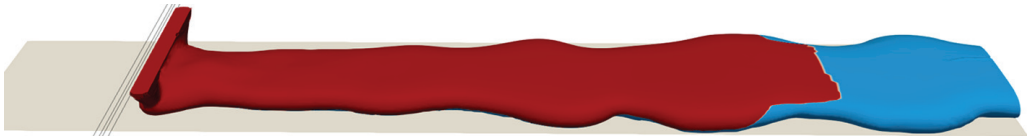

Fig. 6. Phases at $t = 2$ s with the AC field, current $I = 1$ kA, frequency $f = 4$ kHz; red – liquid, blue – solid.

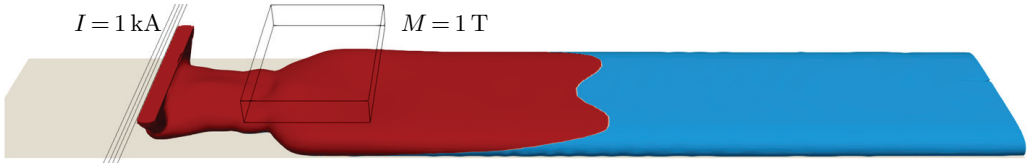

Fig. 7. Phases at steady state with the combined AC ($I = 1$ kA, $f = 4$ kHz) and static magnetic field ($M_y = M_0 = 1$ T); red – liquid, blue – solid.

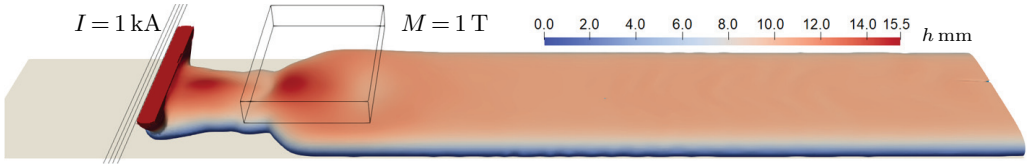

Fig. 8. Layer thickness at steady state with the combined AC ($I = 1$ kA, $f = 4$ kHz) and static magnetic field ($M_y = M_0 = 1$ T).

A representative phase distribution at a later time is shown in Fig. 6.

The AC field solves the back-flow problem, but overall makes the cast strip more non-uniform. Surface oscillations can be stabilized by a static (or traveling) magnetic field. We test this by placing a source of static vertical magnetic field (magnetization $M_y = M_0 = 1$ T) above the section, where most of the liquid metal is flowing faster than the belt, as evidenced by the narrowing of the melt layer. Figs. 7 and 8 show the phases and layer thickness during stable casting with the combined AC ($I = 1$ kA, $f = 4$ kHz) and static magnetic field ($M_y = M_0 = 1$ T). The melt is abruptly slowed down by the static field forcing it to distribute across the belt.

With the intensive belt cooling, a small amount of the melt immediately solidifies upon contact with the belt. Fig. 9 shows the phase distribution in different cross-sections with the combined AC and static field. The part of the melt that solidifies right at the contact with the belt is constantly being remelted by the incoming hot liquid metal and by the recirculation in this zone.

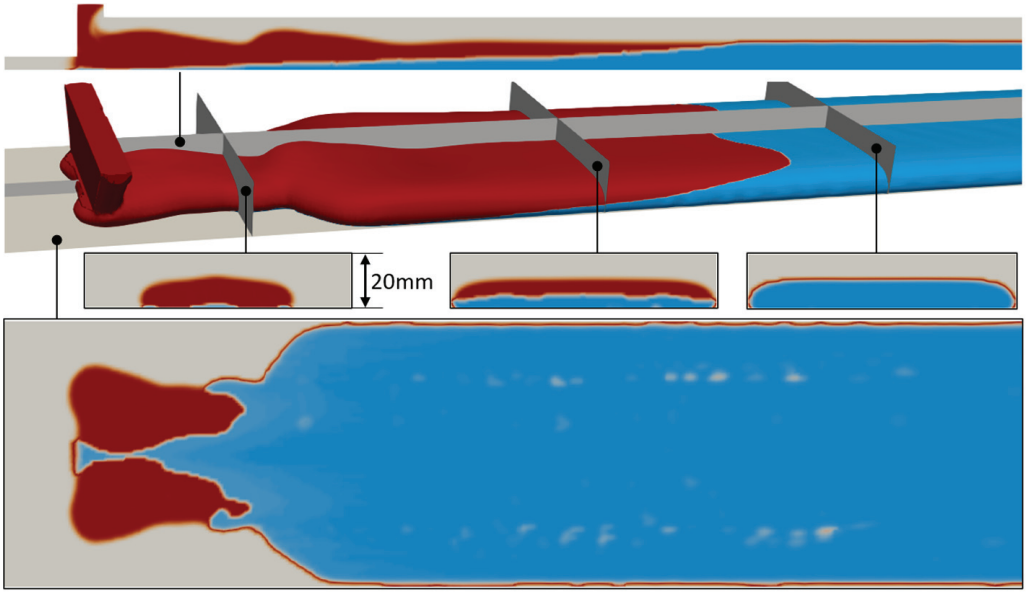

Fig. 9. Phases in different cross-sections with the combined AC ($I = 1\,\text{kA}$, $f = 4\,\text{kHz}$) and static field ($M_y = M_0 = 1\,\text{T}$); red – liquid, blue – solid, grey – gas.

The two streaks of brighter spots at the bottom in Fig. 9 indicate bubble entrapment. This is characteristic to the belt casting process, as reported in [12],[2]. In our model, the bubble entrapment occurs at the zones, where the melt suddenly expands across the belt due to the EM braking by the static magnetic field. Gas entrapment is detrimental not only due to the formation of cavities, but gas bubbles decrease the heat fluxes at those spots. Since in our model the heat flux is fixed, the bubbles have very little effect on the heat transfer.

Conclusions.

This work presents simulations of the direct strip casting process with EM control. AC magnetic field of a straight inductor placed near the gap was proved to be very efficient in completely preventing the back-flow. The edge instabilities observed in our previous work do not appear to have much influence. However, some surface oscillations cause non-uniformities of the strip profile downstream. Combining AC field for back-flow and static field for surface stabilization appears to completely stabilize the casting process.

While the results demonstrate a possible solution to stability problems in the belt casting process, they should be taken only qualitatively due to several assumptions and simplifications in the model, such as constant material properties and ignored thermal radiation. Moreover, we studied this process in a relatively small system. The industrial scale can be considerably larger, which means that the process could be more unstable, which would require adaptation and optimization of the EM parameters. Further work is needed to assess the influence of the assumptions and simplifications in the model, as well as to investigate the application of these solutions on an industrial scale.

Acknowledgements. The work was partially supported financially by the ERDF project No. 1.1.1.1/18/A/108 “Development of numerical modelling approaches to study complex multiphysical interactions in electromagnetic liquid metal technologies” and by

the ESF project No. 8.2.2.0/20/I/006 “Strengthening the capacity of the UL PhD programme in the new doctoral model”.

References

[1] U. Niaz. Numerical modeling and experimental casting of aa6111 aluminium alloy and advanced high strength steels (ahss) produced through horizontal single belt casting (hsbc) process. (Ph.D. thesis, McGill University, Canada), 2020.

[2] S. Ge. Numerical and physical modeling of the horizontal single belt casting (hsbc) process. Ph.D. thesis, McGill University, Canada, 2015.

[3] K. H. Spitzer, *et al.* Direct strip casting (dsc) – an option for the production of new steel grades. *Steel Research International*, vol. 74 (2003), pp. 724–731.

[4] U. Niaz, M. M. Isac, and R.I.L. Guthrie. Numerical modeling of transport phenomena in the horizontal single belt casting (hsbc) process for the production of aa6111 aluminum alloy strip. *Processes*, vol. 8 (2020), p. 529.

[5] J. S. Kim, M. Isac, and R.I.L. Guthrie. Metal-mold heat transfer and solidification of magnesium alloys in belt casting processes. In *TMS Annual Meeting* (2004), pp. 247–255.

[6] H. Palkowski and L. Wondraczek. Direct strip casting of magnesium. *International Journal of Materials Research*, vol. 95 (2004), pp. 1080–1086.

[7] J. Wans, *et al.* Belt casting technology - experiences based on the worldwide first bct caster. In *46º Seminário de Aciaria – Internacional* (2015).

[8] R.I.L. Guthrie and M. Isac. Continuous casting practices for steel: Past, present and future. *Metals*, vol. 12 (2022), p. 862.

[9] C. Klinkenberg, B. Kintscher, K. Hoen, and M. Reifferscheid. More than 25 years of experience in thin slab casting and rolling current state of the art and future developments. *Steel Research International*, vol. 88 (2017), p. 1700272.

[10] S. Ge, M. Isac, and R.I.L. Guthrie. Progress in strip casting technologies for steel; technical developments. *ISIJ International*, vol. 53 (2013), pp. 729–742.

[11] J. Kroos, *et al.* Development of the direct strip casting process. (2003). EC Report 20598: https://op.europa.eu/en/publication-detail/-/publication/f737caf3-4071-49fc-b616-2d45e6f46df8.

[12] S. Ge, M. Isac, and R.I.L. Guthrie. The computational fluid dynamic (cfd) modeling of the horizontal single belt casting (hsbc) processing of Al-Mg-Sc-Zr alloy strips. *Metallurgical and Materials Transactions B*, vol. 46 (2015), p. 2264–2277.

[13] M. McBrien, J.M. Allwood, and N.S. Barekar. Tailor blank casting - control of sheet width using an electromagnetic edge dam in aluminium twin roll casting. *Journal of Materials Processing Technology*, vol. 224 (2015), pp. 60–72.

[14] V. Dzelme, A. Jakovičs, and E. Baake. Dynamics of liquid metal layer in transverse ac magnetic field. *Magnetohydrodynamics*, vol. 58 (2022), pp. 141–150.

[15] Elmer FEM, https://www.csc.fi/web/elmer.

[16] OpenFOAM, https://openfoam.org.

[17] J. Venčels, P. Raback, and V. Geža. Eof-library: Open-source elmer fem and openfoam coupler for electromagnetics and fluid dynamics. *SoftwareX*, vol. 9 (2019), pp. 68–72.

[18] V. Dzelme, A. Jegorovs, and A. Jakovičs. Liquid metal free surface dynamics in rotating permanent magnet stirrer. *IOP Conference Series: Materials Science and Engineering*, vol. 950 (2020), p. 012018.

[19] R. Baranovskis, *et al.* Contactless aluminum degassing system – GaInSn model experiments and numerical study. *Journal of Sustainable Metallurgy*, vol. 7 (2021), pp. 1899–1909.

[20] J. Venčels, A. Jakovičs, and V. Geža. Simulation of 3d mhd with free surface using open-source eof-library: levitating liquid metal in an alternating electromagnetic field. *Magnetohydrodynamics*, vol. 53 (2017), pp. 643–652.

[21] N. Sizganov and M. Khatsayuk. Free metal surface resonance under alternating magnetic field low-frequency oscillations. *IOP Conf. Series: Materials Science and Engineering*, vol. 950 (2020), p. 012010.

[22] V. Geža, J. Venčels, G. Zāģeris, and S. Pavlovs. Numerical study of surface waves generated by low frequency em field for silicon refinement. *IOP Conf. Series: Materials Science and Engineering*, vol. 424 (2018), p. 012049.

[23] M. Leitner, *et al.* Thermophysical properties of liquid aluminum. *Metallurgical and Materials Transactions A*, vol. 48 (2017), pp. 3036–3045.

[24] C.W. Hirt and B.D. Nichols. Volume of fluid (vof) method for the dynamics of free boundaries. vol. 39 (1981), p. 201–225.

[25] F. Rosler and D. Bruggemann. Shell-and-tube type latent heat thermal energy storage: numerical analysis and comparison with experiments. *Heat and Mass Transfer*, vol. 47 (2011).

Received 02.01.2024